# Phoamtonic designs yield sizeable 3D photonic band gaps

**Michael A. Klatt[a,1], Paul J. Steinhardt[a,1], and Salvatore Torquato[a,b,c,d,1]**

[a]Department of Physics, Princeton University, Princeton, NJ 08544; [b]Department of Chemistry, Princeton University, Princeton, NJ 08544; [c]Princeton Institute for the Science and Technology of Materials, Princeton University, Princeton, NJ 08544; and [d]Program in Applied and Computational Mathematics, Princeton University, Princeton, NJ 08544

Edited by David A. Weitz, Harvard University, Cambridge, MA, and approved October 7, 2019 (received for review July 23, 2019)

**We show that it is possible to construct foam-based heterostructures with complete photonic band gaps. Three-dimensional foams are promising candidates for the self-organization of large photonic networks with combinations of physical characteristics that may be useful for applications. The largest band gap found is based on 3D Weaire–Phelan foam, a structure that was originally introduced as a solution to the Kelvin problem of finding the 3D tessellation composed of equal-volume cells that has the least surface area. The photonic band gap has a maximal size of 16.9% (at a volume fraction of 21.6% for a dielectric contrast $\varepsilon = 13$) and a high degree of isotropy, properties that are advantageous in designing photonic waveguides and circuits. We also present results for 2 other foam-based heterostructures based on Kelvin and C15 foams that have somewhat smaller but still significant band gaps.**

Plateau's laws for dry foam | Weaire–Phelan foam | TCP structures and Frank–Kasper phases | self-organization | complete photonic band gap

Foams are both of fundamental interest (1) and important for a host of applications ranging from chemical filters to heat exchangers (2). They locally minimize the surface area of their cells subject to volume constraints. In the limit of vanishing liquid fraction, the so-called dry foam is completely characterized by Plateau's laws, where each cell vertex is tetrahedral; that is, 4 edges meet with bond angles equal to $\arccos(-1/3) \approx 109^\circ$. These laws were first observed empirically (3) and later proven rigorously for area-minimizing tessellations with volume constraints (4, 5).

Kelvin posed the fundamental question: What tessellation with cells of equal volume has the least surface area? He conjectured that the solution is a relaxation of the Voronoi tessellation of the body-centered cubic (BCC) lattice—now known as the Kelvin foam (1). More than 100 y later, Weaire and Phelan disproved the conjecture by finding a foam with a slightly smaller surface area (6). Their numerical finding was later rigorously confirmed (7). The Weaire–Phelan foam can be obtained by relaxing a weighted Voronoi tessellation of the A15 crystal. Importantly, the foam has been not only studied numerically (8) but also realized experimentally (9). Whether it is the globally optimal solution to Kelvin's problem is still an open question. The Weaire–Phelan foam has 2 types of cells with different pressures. So the Kelvin foam has still the least surface area among known foams with equal pressure in each cell. Kelvin cells have also been found in experiments (10–12). The A15 crystal ($\beta$-tungsten) belongs to a larger class of so-called tetrahedrally close-packed (TCP) structures (or Frank–Kasper phases) (13). This class includes, for example, the C15 crystal (cubic Friauf–Laves phase). Relaxing its Voronoi diagram, subject to the constraint that each cell has the same volume, defines the C15 foam (14). Its surface area is larger than that of the Kelvin foam. Here we study these 3 foams—Weaire–Phelan, Kelvin, and C15—as classic examples of crystalline foams. Their electrical, mechanical, and transport properties have been intensively studied elsewhere (15–21).

In this paper, we consider phoamtonics, the potential application of these foam-based architectures to photonic materials. For this purpose, the essential question is whether the resulting materials have complete photonic band gaps (PGBs) that prohibit the propagation of light in all directions and for all polarizations for a substantial range of frequencies. If so, they would expand the range of 3D heterostructures available for photonic applications beyond photonic crystals (22–24), quasicrystals (25–27), and amorphous networks (28–30).

Here we demonstrate that a 3D photonic network based on the Weaire–Phelan foam results in a substantial complete PBG (16.9%) with a high degree of isotropy, an important property for photonic circuits. We find substantial PBGs for the Kelvin and C15 foam, but the Weaire–Phelan network has the largest phoamtonic band gap. This provides impetus for further studies of foam-based photonic materials.

There are 2 motivations for phoamtonics. First, Plateau's laws guarantee exclusively tetrahedral vertices. The latter are generally thought to be advantageous for photonic networks, as explained below. This naturally relates photonics to the Kelvin problem, that is, the search for the 3D tessellation composed of equal-volume cells that has the least surface area—a problem of fundamental interest in both mathematics and physics. Its connections to famous packing and covering problems (31) relate foams, for example, to Frank–Kasper phases (6, 14, 32–34) and their dual clathrate structures (35–37). The self-assembly* of

PHYSICS

## Significance

**Foams appear ubiquitously in many fields of science and technology. However, applications to photonics have not been possible because until now, foam-based 3D heterostructures with substantial complete photonic band gaps have not been identified. Here we provide explicit examples based on the edges of dry-crystalline foams, including the famous Weaire–Phelan foam. More generally, foam networks based on Frank–Kasper phases offer new, promising approaches to the rapid self-organization of large photonic networks. Moreover, foams are excellent candidates for designer materials with versatile multifunctional characteristics.**

Author contributions: M.A.K., P.J.S., and S.T. designed research; M.A.K., P.J.S., and S.T. performed research; M.A.K. analyzed data; and M.A.K., P.J.S., and S.T. wrote the paper.

The authors declare no competing interest.

This article is a PNAS Direct Submission.



Data deposition: All data generated or analyzed for this study, including configurations, parameter files, raw output, and postprocessed data, are available at the Zenodo repository, https://zenodo.org/, as Databases 1–3 (DOI: 10.5281/zenodo.3401635).

[1]To whom correspondence may be addressed. Email: mklatt@princeton.edu, steinh@princeton.edu, or torquato@princeton.edu.

This article contains supporting information online at www.pnas.org/lookup/suppl/doi:10.1073/pnas.1912730116/-/DCSupplemental.

*In this paper, we apply the term "self-assembly" to equilibrium systems, whereas "self-organization" also refers to athermal or nonequilibrium systems.

Frank–Kasper phases in soft-matter systems has recently sparked great interest (38). Second, the utility of foams for applications is proven by their widespread use in technology. Particularly promising for photonics are their self-organization, multifunctionality, and a high degree of isotropy among crystal structures.

Recently, Ricouvier et al. (39) studied 2D dry and wet foams as a self-organizing PBG material. These authors demonstrated that 2D amorphous dry foams exhibit PBGs only for transverse electric polarization. They found that the PBG is incomplete for the transverse magnetic polarization. The authors suggested continuing the quest for a complete PGB by considering foams in 3D. This is a nontrivial endeavor: dimensionality dramatically changes the picture because in 3D, there are 2 polarizations that couple, in contrast to 2D. Nevertheless, stimulated by their suggestion, we pursued the 3D case and found that 3D foam-based heterostructures with substantial complete PBGs are possible.

A reason why one might consider 3D foams to be promising as photonic materials is that Plateau's laws guarantee that the edges form exclusively tetrahedral vertices. The latter are well known to be favorable for photonic networks (24, 30, 40). For example, the network with the largest PBG of about 30% is the diamond crystal (40), where the gap size is measured by the ratio of the frequency width $\Delta\omega$ of the gap and the midgap frequency $\omega_m$. (Unless otherwise stated, we always cite gap–midgap ratios for a dielectric contrast of 13 to 1 and a volume fraction of the high dielectric material that maximizes the gap.) The hexagonal diamond network also has exclusively tetrahedral bonds but a different crystal structure resulting in a PBG of about 23%. On the one hand, these 2 examples demonstrate that the global geometry and topology are important factors in addition to having purely local tetrahedral bonds. On the other hand, they also suggest that networks with tetrahedral bonds are advantageous for photonics, perhaps because they enable a high degree of on-average isotropy or self-uniformity (30, 41).

Foams share the tetrahedral coordination property of the diamond lattice, but they differ in having curved edges and somewhat unequal bond lengths. One of the reasons to explore foam-based networks is to determine the degree to which these differences change their photonic properties. The key result presented here is that the differences are not sufficient to prohibit a substantial complete PBG, even if the size is reduced by half compared to the diamond crystal.

By thickening the edges of 3D crystalline dry foams, we create photonic networks, shown in Fig. 1, that exhibit pronounced photonic PBGs of up to 17%, comparable to or exceeding those of typical examples of self-organizing photonic crystals like geometrically optimized synthetic opals (42). To experimentally realize such thickened edges, a dry foam needs to be first solidified and then coated by a dielectric material as recently suggested by Ricouvier et al. (39). In fact, a similar procedure has already been used to convert a 3D polymer network into a photonic silicon-coated network with $\mathrm{TiO_2}$ cores designed for infrared wavelengths (43).

The somewhat reduced PBG compared to diamond photonic crystals may be compensated by the additional advantages of phoamtonics compared to other photonic materials. For example, the self-organization of foams may allow for rapid fabrication of large samples. Also, due to the extensive previous studies of the physical properties of foams, such as their stiffness and conductivity (15–18), photonic foam-based heterostructures may be excellent candidates for certain multipurpose applications. Furthermore, as we will demonstrate, Weaire–Phelan and C15 networks have complete PBGs that are nearly isotropic, which is useful for applications ranging from highly isotropic and efficient thermal radiation sources (44) to more adjustable bending angles in waveguides (27, 45, 46) and photonic circuits.

## Geometry and Topology of Foam Edges

Here we study dry foams that are defined as local minima of the interfacial area of a tessellation subject to volume constraints such that the final geometry obeys Plateau's laws (3, 5, 32). To construct the Weaire–Phelan, Kelvin, or C15 foams, we start from suitably weighted Voronoi tessellations (7) of the BCC, A15, or C15 crystals, respectively. The weights are chosen such that each cell has the same volume. Using Ken Brakke's Surface Evolver (47), we minimize the surface area subject to the constraint that the equal volumes are fixed; for details, see *Precise Foam Approximants*. Due to the scale invariance of Maxwell's equations, the unit of length $a$ can be chosen freely for photonic calculations. Here we choose it such that the number of vertices per primitive unit cell is equal to its volume; that is, the networks are compared at the same density of vertices (average number per unit volume).

We study both networks formed by the curved edges of the foams and those formed by the straight edges of their progenitor tessellations. First, we use ring statistics to analyze their topology. More precisely, we count the number of shortest rings (48) per vertex in the primitive unit cell; for more details, see *SI Appendix*. In the examples studied here, the topology of a foam is equivalent to that of its progenitor tessellation, and the shortest rings

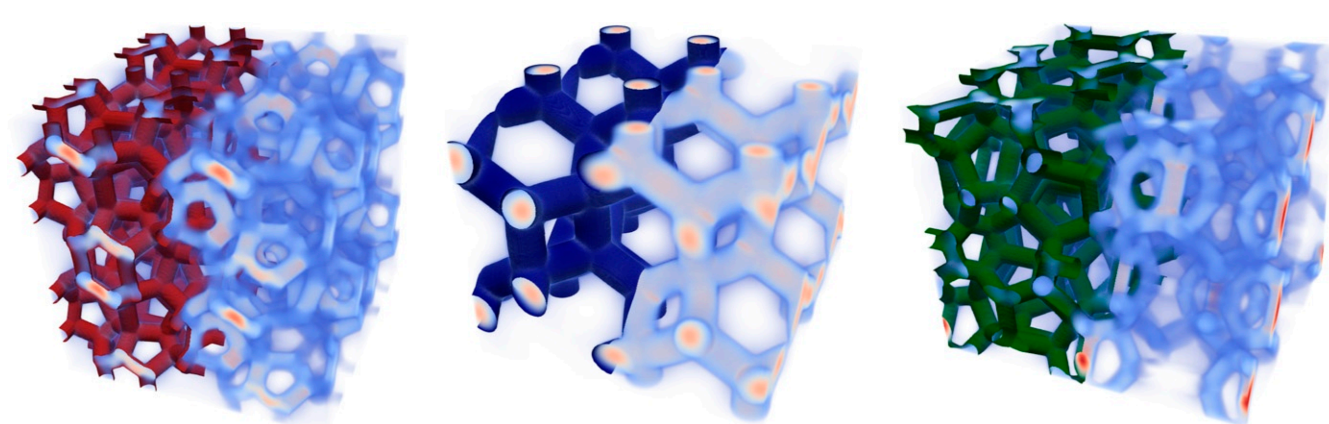

**Fig. 1.** Phoamtonic networks in 3D obtained by thickening the edges of crystalline Weaire–Phelan foam (*Left*), Kelvin foam (*Center*), and C15 foam (*Right*): for each crystal, $2 \times 2 \times 2$ cubic unit cells are shown. Each sample depicts a portion of the network and the time-averaged electric-field energy density of a mode at $\Gamma$ in the highest dielectric band (HDB, which is the highest band below the gap). For more modes, see Movies S1–S3. The dielectric contrast is $\varepsilon = 13$, and the volume fractions are 21.7, 19.6, and 18.8%.

coincide with the faces of the cells. While a Kelvin cell has 2 squares and 4 hexagons per vertex, the TCP foams have only pentagonal and hexagonal faces (on average, 5.2 and 0.78 in the Weaire–Phelan foam and 5.3 and 0.71 in the C15 foam), which may be related to their importance for foams (32). The A15 and C15 Voronoi tessellations are the TCP structures with the most or least average number of faces $\bar{f}$ per cell (32). The Weaire–Phelan structure has the largest value of $\bar{f} = 13 + 1/2$, and the C15 structure has the smallest $\bar{f} = 13 + 1/3$.

In the relaxed foam, Plateau's rules guarantee that each vertex has valency 4 and that the incident bond angle between any 2 edges is $\arccos(-1/3) \approx 0.608\pi \approx 109^\circ$. While the first statement also holds for the progenitor tessellations, the second must be violated by a tessellation with flat faces (32).

For the A15, C15, and BCC lattice, the distributions of bond lengths and angles in the weighted Voronoi diagrams with straight edges are plotted in *SI Appendix*, Fig. S1. Detailed statistics of the bond length and angle distributions of both the foams and their progenitors are listed in *SI Appendix*, Table S2.

All edges of the BCC Voronoi diagram have exactly the same length, in contrast to those in the TCP structures. There is less variation in the A15 (18.5%) than in the C15 structure (26.3%). The variance of bond lengths decreases for the relaxed foams (14.7 and 24.7%) with curved edges.

The average of the bond angles in the BCC Voronoi tessellation differs from the tetrahedral angle by about 0.5%. For the A15 and C15 crystals, the average bond angles are an order of magnitude closer to the tetrahedral value with differences of about 0.09 and 0.06%, respectively. In that sense, the weighted Voronoi diagrams of the A15 and C15 crystals have effectively tetrahedral bond angles. Moreover, the standard deviations of their bond angles are smaller than those of the BCC lattice (*SI Appendix*, Table S2).

## Phoamtonic Networks

Next, we construct a photonic network based on the edges of dry foam. Its volume fraction $\phi$ is the fraction of volume covered by the high dielectric material. Typical values of $\phi$ that maximize the PBG are about 20% (49). The Weaire–Phelan foam becomes unstable at about 15% volume fraction (8). So we do not consider wet foam, where the Plateau borders have tricuspoid cross sections. Instead, we start from dry foam structures and homogeneously thicken each edge. Each edge is finally the medial axis of a spherocylinder, where the radius is a tuning parameter. Such a foam-based network is not literally a foam, but for simplicity we will henceforth refer to heterostructures derived from foams in this way as "foams" or "foam networks." Fig. 1 illustrates these 3D networks.

For an accurate prediction of the photonic band structure, we solve the frequency-domain eigenproblem with the plane-wave expansion method implemented in the Massachusetts Institute of Technology (MIT) Photonic Bands (MPB) software package (50). To achieve high numerical precision, we choose a high resolution of the discretization, a low tolerance of the eigensolver, and a high sampling of the $k$-points; for more details, see *Creating and Analyzing Phoamtonic Networks*. Using primitive unit cells and the standard notation for high-symmetry $k$-points of the Brillouin zone, we choose paths along the boundary of the irreducible Brillouin zones similar to those in ref. 51.

The dielectric contrast $\varepsilon$ is the ratio of the dielectric constants of the high- to low-dielectric material (24). Unless otherwise stated, we assume a dielectric contrast of 13 to 1, which is commonly used in the literature as a standard when comparing the performance of different photonic material designs (28, 30, 40). To facilitate experimental realizations, our map of gap sizes below shows the gap–midgap ratios at lower dielectric contrast. For each network, the radius of the edges (spherocylinders) is optimized for a maximal gap–midgap ratio $\Delta\omega/\omega_m$, where $\Delta\omega$ is the frequency width of the gap (the difference between the lowest-frequency eigenvalue in the lowest air band and the highest in the HDB), and $\omega_m$ is the frequency at the middle of the gap. The radii that maximize the gap–midgap ratio differ by a few percent, and so does the corresponding volume fraction covered by the network; for more details, see *SI Appendix*, Table S3.

For the Weaire–Phelan, Kelvin, and C15 foam networks, the photonic band structures are shown in Figs. 2–4. Time-averaged electric-field energy densities of modes in the HDBs are depicted together with small portions of the 3D networks in Fig. 1. More energy densities are presented in Movies S1–S3.

The same analysis is repeated for 4 classic photonic crystals: the diamond, Laves, hexagonal diamond, and simple cubic networks. Their photonic band structures are depicted in *SI Appendix*, Figs. S2–S5.

**Gap Sizes.** The PBG sizes, measured by the gap–midgap ratio $\Delta\omega/\omega_m$, are 7.7% for the Kelvin foam, 13.0% for the C15 foam, and 16.9% for the Weaire–Phelan foam. The minimization of the surface area increases the gap size by 0.7, 0.3, or 1.3%, that is, comparing the progenitor tilings with straight edges and slightly nonuniform vertices to the relaxed foams with curved edges and tetrahedral vertices. The gap edges are listed in *SI Appendix*; for further details, see also *SI Appendix*, Table S3.

The TCP foam networks with effectively tetrahedral bond angles have distinctly larger gap sizes than the Kelvin network. Between the 2 TCP structures, the Weaire–Phelan network has the larger gap size, presumably due to the smaller variation in bond lengths. The Weaire–Phelan foam has not only the currently smallest known interfacial area; its corresponding network also has the largest PBG.

Perhaps due to the variations in bond lengths, the gap sizes of our foam-based photonic networks are as expected smaller than the largest known gaps, which are found in networks based on the diamond (31.6%) and Laves (28.3%) graph; for more details and other classic networks, see *Classic Photonic Crystals* and, e.g., refs. 24, 30, 40, and 49.

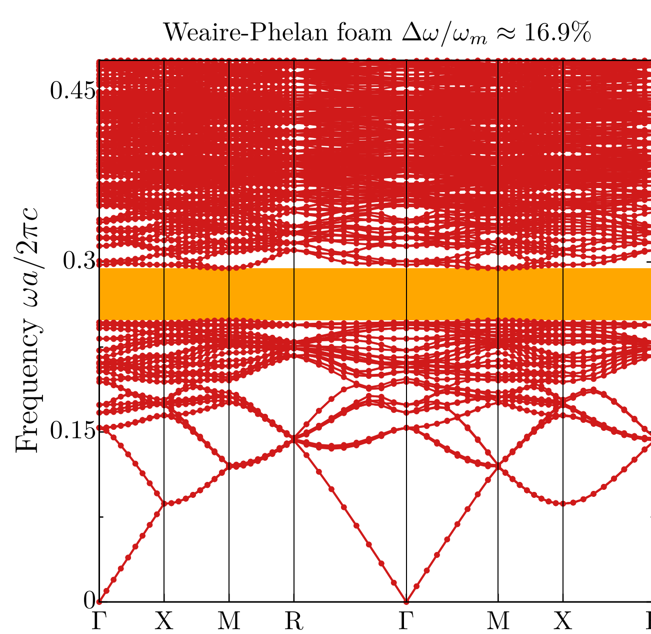


**Fig. 2.** Photonic band structure for the Weaire–Phelan foam in a cubic primitive unit cell at a dielectric contrast $\varepsilon = 13$ and a volume fraction $\phi = 21.7\%$. For a 3D sample, see Fig. 1 (*Left*).

PHYSICS

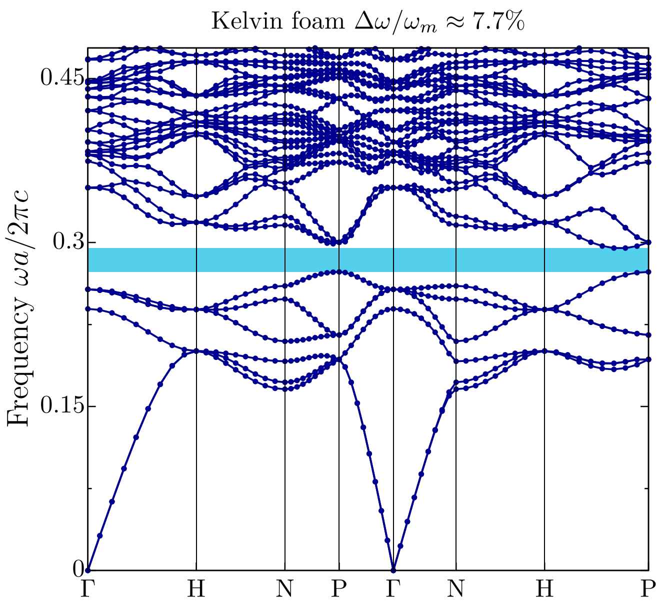


**Fig. 3.** Photonic band structure for the Kelvin foam in a primitive unit cell of a body-centered cubic crystal at a dielectric contrast $\varepsilon = 13$ and a volume fraction $\phi = 19.6\%$. For a 3D sample, see Fig. 1 (*Center*).

**Gap Isotropy.** Isotropic PBGs are highly advantageous in photonic applications because they enable freeform waveguides and flexible circuit design (27, 46). Photonic quasicrystals as well as amorphous photonic networks (elaborated on in the discussion) are more isotropic than classic photonic crystals (25, 26, 46, 52).

Here we show that phoamtonic band gaps also have a high degree of isotropy. Different metrics for isotropy of PBGs have been proposed (26, 52). Effects from the folding of bands for complex unit cells can largely be avoided by restricting the anisotropy analysis to the boundary of the Brillouin zone (26). We quantify the variations of the bands at the boundary of the Brillouin zone that corresponds to the primitive unit cell. An intricate reconstruction of the dispersion relation via experimental or simulated measurements of transmission and phase delay (52) is beyond the scope of this study.

Here we define the gap anisotropy index $\mathcal{A}$ that captures variations of the PBG at the edge of the Brillouin zone (given a primitive unit cell):

$$\mathcal{A} := \sqrt{\mathbb{V}\mathrm{ar}[\omega_{\mathrm{HDB}}] + \mathbb{V}\mathrm{ar}[\omega_{\mathrm{LAB}}]}/\omega_m,$$

where $\omega_{\mathrm{HDB}}$ and $\omega_{\mathrm{LAB}}$ are the eigenfrequencies of the highest dielectric and lowest air band, illustrated in Movie S4. See *SI Appendix* for a precise definition of the variance $\mathbb{V}\mathrm{ar}[.]$ and its estimator.

The C15 foam is found to have the lowest anisotropy index (1.0%), very closely followed by the Weaire–Phelan foam (1.2%). So the TCP foams provide the possibility of self-organizing photonic networks with remarkably isotropic PBGs.

The gap of the Kelvin foam is distinctly more anisotropic (3.5%), which is similar to the Laves network (3.4%) and the diamond network (4.2%). These networks are still comparably isotropic relative to the simple cubic (8.8%) and hexagonal diamond (9.7%) networks. Note that the relative isotropy of the diamond at the boundary of the Brillouin zone is commonly understood as one of the reasons for its excellent photonic properties.

**Maps of Gap Sizes.** Applications seeking a trade-off between different physical properties generally require deviations from the rod radii that maximize the PBG of the network. For example, at small volume fractions $\phi$, the stiffness of solid foams (i.e., their shear modulus) increases with $\phi$ (16). Moreover, different techniques of self-organization might have restrictions to the dielectric contrast $\varepsilon$.

In an extensive numerical study, we have therefore computed the photonic gap–midgap ratio as a function of $\varepsilon$, where for each value we have separately optimized the radius to maximize $\Delta\omega/\omega_m$. For $\varepsilon = 13$, we have varied the volume fraction $\phi$, which we estimate by the dielectric filling fraction as defined in *SI Appendix*. Fig. 5 compares the gap sizes of the foams to those of the diamond network and other prominent photonic crystals; see *SI Appendix* for more details. Fig. S6 shows 3D maps of gap sizes, that is, $\Delta\omega/\omega_m$ as a function of both $\varepsilon$ and $\phi$.

The Weaire–Phelan foam supports reasonable gap sizes of about 8% down to a dielectric contrast $\varepsilon \approx 9$, where the radius with the maximal PBG increases by about 15%. The PGB vanishes for $\varepsilon < 6.5$. As expected, the diamond network has the largest gap for all dielectric contrasts.

All networks are relatively insensitive to the volume fraction. For the Weaire–Phelan foam, PBGs of about 8% (at $\varepsilon = 13$) persist down to half of the value that maximizes the gap–midgap ratio. At these volume fractions, a wet Weaire–Phelan foam is stable. So its solidification can, in principle, directly lead to a photonic network, although this remains to be confirmed by computing the band structure for a network with Plateau borders (with a tricuspoid as cross section).

## Discussion and Outlook

Motivated by the connection between Plateau's laws and known preferential geometries of photonic networks, we positively answered the question of whether foam networks can exhibit complete PBGs. Converting the edges of crystalline dry foams into photonic networks, we found pronounced PBGs. They are smaller than for the diamond network but larger than in typical self-organizing systems. The fairly isotropic PBGs of our phoamtonic networks are advantageous for photonic circuit and waveguide design.

One of the motivations for studying the crystalline foams described in this paper is to identify characteristics that may

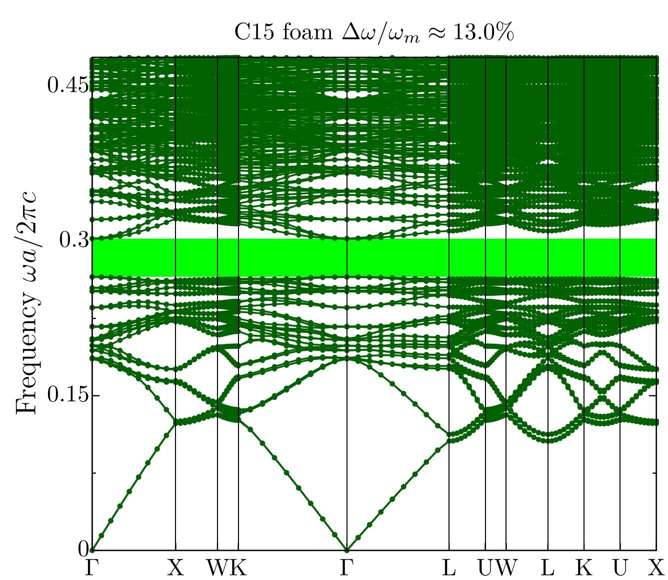


**Fig. 4.** Photonic band structure for the C15 foam in a primitive unit cell of a face-centered cubic crystal at a dielectric contrast $\varepsilon = 13$ and a volume fraction $\phi = 18.8\%$. For a 3D sample, see Fig. 1 (*Right*).

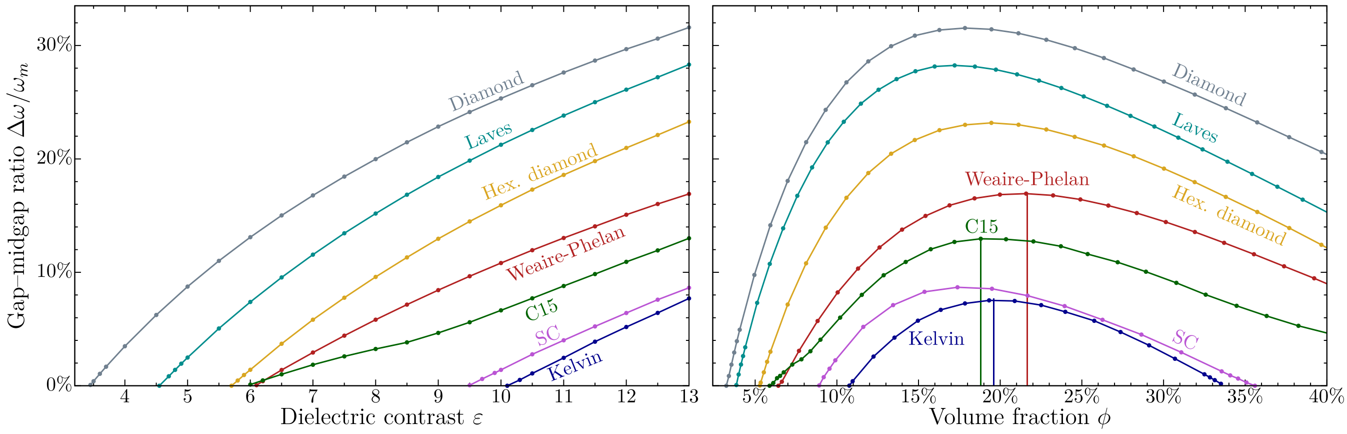


**Fig. 5.** Maps of gap sizes: gap–midgap ratio $\Delta\omega/\omega_m$ as a function of (*Left*) the dielectric contrast, where the radii are optimized at each value of $\varepsilon$ to maximize $\Delta\omega/\omega_m$ [for precise values, see Database S1 (53)], and (*Right*) the volume fraction at a dielectric contrast $\varepsilon = 13$. The vertical lines indicate the maximal gap sizes shown in Figs. 2–4. For more details on the other photonic crystals, see *SI Appendix*. For 3D maps of gap sizes, see Fig. S6.

apply to amorphous foams in 3D. To date, complete band gaps in amorphous networks have only been demonstrated for relatively small systems and are not guaranteed to persist as the system is made larger (30). Amorphous foams are interesting candidates because they would have the advantages of perfect isotropy and tetrahedral bond angles. In addition, they may have less constraining conditions for manufacture compared to crystalline foams. On the other hand, the bond length distribution is much broader than for crystalline foams. At present, the only examples of amorphous networks in 3D (including foams) have either no complete PBGs or PBGs that may not persist in the limit of large system sizes; see, for example, ref. 30. We are currently using the successful experience with Weaire–Phelan foams to guide us in constraining the constructing of amorphous foam heterostructures that will have robust complete PBGs.

**Utilizing Phoamtonics.** Exciting prospects of phoamtonics for applications are 1) the self-organization of photonic networks and 2) the flexible trade-off between physical properties. Importantly, the gap size of the Weaire–Phelan network exceeds that of geometrically optimized synthetic opals and other typical examples of manmade[†] self-organizing large-scale photonic crystals ($<15\%$ at $\varepsilon = 13$) as reported in ref. 42.

Self-assembly of crystal structures that correspond to the Kelvin or Weaire–Phelan foam as well as to other Frank–Kasper phases have recently been reported in a growing list of soft-matter systems; see ref. 38 and references therein. Phoamtonics might thus help with the self-organization at various length scales and offer new opportunities to the recent progress and remaining challenges of the self-assembly of photonic nanomaterials (56, 57). Particularly interesting is the connection between foams and self-assembling supramolecular micellar materials or block-copolymers (38, 58). An alternative approach could use the self-assembly of emulsions (37), e.g., with suitably patchy droplets and emulsion templating for the fabrication of open-cell foams.

We envisage that phoamtonics may be an effective way of fabricating large photonic network solids for applications involving longer wavelengths, such as THz (59, 60) and X band radiation (61). These bands require cell sizes in the millimeter or submillimeter regime, where standard techniques of solid open-cell foams might be highly useful for the fabrication of extended photonic networks. Applications at visible wavelengths are more challenging with current technology.

**Multifunctionality of Foams.** Foams provide an excellent class of multifunctional materials that provide a good trade-off between a number of different physical properties. Phoamtonics thus offers versatile solutions for multipurpose technologies that require further optimizations besides a maximal PBG. Foams are particularly promising lightweight materials because other favorable properties have already been explored, identified, and utilized for a broad spectrum of technologies (2). Besides elastic moduli (17) and conductivities (18, 62), these include, for example, phononic band structures (19), heat transfer (21), diffusive transport of photons (20), or the mechanical strength of metallic foams (63–65).

The elastic properties of 3D networks based on foams, in particular the Weaire–Phelan foam, have been intensively studied as exemplary cellular structures; e.g., see ref. 16. At low volume fractions, the mechanical properties of the Kelvin foam, its bulk and shear moduli, are almost isotropic (within a few percent) in the small strain range (15, 17, 66). They are exactly isotropic for circular cross sections and zero Poisson's ratio (bulk material) (15). At finite volume fractions, the shear moduli of the Kelvin foam are more anisotropic than those of the Weaire–Phelan and C15 foams (16). The average shear moduli are comparable, but the TCP foams are perceptibly stiffer (16). The Young's moduli have been reported to be more isotropic for the Kelvin than for the Weaire–Phelan network (67).

Further intriguing insights were gained for the effective foam conductivity, both in the dry limit (2, 18, 62) and at higher volume fractions (68, 69). Starting from the Lemlich formula (62), Durand et al. (18) found sufficient criteria to maximize the conductivity of a network for a given topology: straight edges and a balancing of the incident directions at each vertex. The latter condition is guaranteed for dry foam by Plateau's laws. Deviations from a maximal conductivity are due to curved edges only. Computing the orientational averaged conductivities of the Kelvin, C15, and Weaire–Phelan foam, Durand et al. (18) found them to be nearly optimal, as expected.

## Materials and Methods

**Classic Photonic Crystals.** We compared the photonic foam networks to 4 classic photonic crystals: diamond, hexagonal diamond, Laves, and simple cubic networks. Hexagonal diamond is also known as Lonsdaleite and closely related to the Wurtzite crystal. The Laves graph (70) is also known as K4 graph (41) or SRS net (71). Its symmetric embedding in Euclidean space is the medial axis of the gyroid, which is a triply periodic minimal surface (71).

[†]Despite recent insights into the formation of biological photonic nanostructures (54, 55), their technological utilization remains a challenge.

PHYSICS

The diamond and simple cubic network also represent the medial axis of 2 other triply periodic minimal surfaces.

The photonic band structures of the 4 networks are shown in *SI Appendix*, Figs. S2–S5. Time-averaged electric-field energy densities in a mode of the band just below the gap (sometimes called the HDB[‡]) are depicted together with small portions of the 3D networks. All energy densities are presented in Movies S5–S8.

**Precise Foam Approximants.** We follow the now common procedure to start with a weighted Voronoi diagram as a progenitor tessellation with flat faces. Keeping the volumes fixed, we minimize the interfacial area using the Surface Evolver (47). The conjugate gradient method is subsequently turned on and off between iterations and refinements of the triangulation. To obtain the network of foam cell edges, edges of triangles are selected according to their valency. For exact parameters and configurations, see *Access to Code and Data*.

**Creating and Analyzing Phoamtonic Networks.** To evaluate the photonic band structure of photonic networks, we used the open-source software MPB (50). In each network, the radius of the edges (i.e., spherocylinders) is constant. We show the gap–midgap ratio as a function of the radius in Fig. 5 (*Right*) and *SI Appendix*, Fig. S6. In all other cases, we optimized the radius to obtain a maximal gap size either by using the function *maximize* based on Brent's algorithm of the LIBCTL library [which in turn is used in MPB (50)] or by manually scanning a range of radii (in particular at low dielectric contrast), as documented in Database S3 (53).

The unit of length was chosen such that the number of vertices per primitive unit cell is equal to its volume, resulting in midgap frequencies $\omega_m$ of about 0.3. The tolerance of the MPB eigensolver was $10^{-7}$, and the mesh size that determines the smoothing of the values of the dielectric constant was 5. The following parameters were used for the high-precision band structures in Figs. 2–4 and Figs. S2–S5: The resolution of the discretization was chosen so that the number of voxels per linear size of each primitive unit cell was more than 70 for the phoamtonic networks, about 60 for the diamond and Laves network, and 40 for the simple cubic network. The frequency eigenvalues were evaluated at all high-symmetry $k$-points of the irreducible Brillouin zone and at 8 intermediate points for each chosen path between these $k$-points as indicated in the band structure plots. For the maps of gap sizes in Fig. 5, we chose a resolution of 24 (number of voxels per unit length). The number of $k$-points varied between the crystals as required. For precise values and data, see *Access to Code and Data*.

Our conservative estimate of the systematic errors is smaller than $1\%$. The main contributions are precision of optimization of the radii, discretization effects, tolerance of the eigensolver, and the approximation of curved edges via segments (decreasingly ordered). The statistical errors of the eigensolver are negligible. Our conservative estimate of the absolute systematic error of the anisotropy index $\mathcal{A}$ is $\mathcal{O}(0.1\%)$, which is mainly caused by systematic errors in the eigenfrequencies and a finite sampling density in the $k$-space (*SI Appendix*).

[‡]In contrast, the lowest air band is just above the gap.

**Access to Code and Data.** The software used in this study, MPB (50) and the Surface Evolver (47), are publicly available on the websites of the projects.

All data generated or analyzed for this study, including configurations, parameter files, raw output, and postprocessed data, are available at the Zenodo repository (53).

Database S1 (53) contains all gap–midgap ratios shown in the maps of gap sizes in Fig. 5 and *SI Appendix*, Fig. S6, together with the corresponding rod radii, volume fractions, or dielectric contrast. The configurations of the networks of edges in both the unrelaxed Voronoi diagrams and the relaxed foams, as well as the classic crystalline photonic networks, are available in Database S2 (53). Database S3 (53) contains all parameters of the photonic calculations, raw output, and postprocessed data.

**ACKNOWLEDGMENTS.** We thank Andy Kraynik for helpful discussions on foams. In particular, we gratefully acknowledge his useful scripts for the Surface Evolver and foam samples. We thank Marian Florescu for insightful discussions on photonics and the MPB software. The simulations presented in this article were substantially performed on computational resources managed and supported by the Princeton Institute for Computational Science and Engineering. This work was supported by the Princeton University Innovation Fund for New Ideas in the Natural Sciences.

1. D. Weaire, *The Kelvin Problem* (Taylor & Francis, London, 1997).
2. L. D. Weaire, S. Hutzler, *The Physics of Foams* (Clarendon Press, Oxford, 1999).
3. J. Plateau, *Statique Expérimentale et Théorique des Liquides Soumis aux Seules Forces Moléculaires* (Gauthier-Villars, Paris, 1873).
4. F. J. Almgren, J. E. Taylor, The geometry of soap films and soap bubbles. *Sci. Am.* **235**, 82–93 (1976).
5. J. E. Taylor, The structure of singularities in soap-bubble-like and soap-film-like minimal surfaces. *Ann. Math.*, **103**, 489–539 (1976).
6. D. Weaire, R. Phelan, A counter-example to Kelvin's conjecture on minimal surfaces. *Philos. Mag. Lett.* **69**, 107–110 (1994).
7. R. Kusner, J. M. Sullivan, "Comparing the Weaire-Phelan equal-volume foam to Kelvin's foam" in *The Kelvin Problem: Foam Structures of Minimal Surface Area*, D. Weaire, Ed. (Taylor & Francis, London, 1996), pp. 71–80.
8. R. Phelan, D. Weaire, K. Brakke, Computation of equilibrium foam structures using the surface evolver. *Exp. Math.* **4**, 181–192 (1995).
9. R. Gabbrielli, A. J. Meagher, D. Weaire, K. A. Brakke, S. Hutzler, An experimental realization of the Weaire–Phelan structure in monodisperse liquid foam. *Philos. Mag. Lett.*, **92**, 1–6 (2012).
10. M. E. Rosa, M. A. Fortes, M. F. Vaz, Deformation of three-dimensional monodisperse liquid foams. *Eur. Phys. J. E* **7**, 129–140 (2002).
11. A. van der Net, G. W. Delaney, W. Drenckhan, D. Weaire, S. Hutzler, Crystalline arrangements of microbubbles in monodisperse foams. *Colloids Surf. A* **309**, 117–124 (2007).
12. R. Höhler, Y. Y. C. Sang, E. Lorenceau, S. Cohen-Addad, Osmotic pressure and structures of monodisperse ordered foam. *Langmuir* **24**, 418–425 (2008).
13. J.-F. Sadoc, R. Mosseri, "Geometrical frustration" in *Collection Alea-Saclay: Monographs and Texts in Statistical Physics* (Cambridge University Press, Cambridge, 1999).
14. N. Rivier, Kelvin's conjecture on minimal froths and the counter-example of Weaire and Phelan. *Philos. Mag. Lett.*, **69**, 297–303 (1994).
15. W. E. Warren, A. M. Kraynik, Linear elastic behavior of a low-density Kelvin foam with open cells. *J. Appl. Mech.* **64**, 787–794 (1997).
16. A. M. Kraynik, M. K. Neilsen, D. A. Reinelt, W. E. Warren, "Foam micromechanics" in *Foams and Emulsions*, J. F. Sadoc, N. Rivier, Eds. (Springer, Dordrecht, The Netherlands, 1999), pp. 259–286.
17. R. M. Christensen, Mechanics of cellular and other low-density materials. *Int. J. Solids Struct.* **37**, 93–104 (2000).
18. M. Durand, J.-F. Sadoc, D. Weaire, Maximum electrical conductivity of a network of uniform wires: The Lemlich law as an upper bound. *Proc. R. Soc. London, Ser. A* **460**, 1269–1284 (2004).
19. A. Spadoni, R. Höhler, S. Cohen-Addad, V. Dorodnitsyn, Closed-cell crystalline foams: Self-assembling, resonant metamaterials. *J. Acoust. Soc. Am.* **135**, 1692–1699 (2014).
20. M. Miri, E. Madadi, H. Stark, Diffusive transport of light in a Kelvin foam. *Phys. Rev. E* **72**, 031111 (2005).
21. S. Cunsolo *et al.*, Lord Kelvin and Weaire–Phelan foam models: Heat transfer and pressure drop. *J. Heat Transf.* **138**, 022601 (2015).
22. E. Yablonovitch, Inhibited spontaneous emission in solid-state Physics and electronics. *Phys. Rev. Lett.* **58**, 2059–2062 (1987).
23. S. John, Strong localization of photons in certain disordered dielectric superlattices. *Phys. Rev. Lett.* **58**, 2486–2489 (1987).
24. J. D. Joannopoulos, S. G. Johnson, J. N. Winn, R. D. Meade, *Photonic Crystals: Molding the Flow of Light* (Princeton University Press, Princeton, ed. 2, 2008).
25. W. Man, M. Megens, P. J. Steinhardt, P. M. Chaikin, Experimental measurement of the photonic properties of icosahedral quasicrystals. *Nature* **436**, 993–996 (2005).
26. M. C. Rechtsman, H.-C. Jeong, P. M. Chaikin, S. Torquato, P. J. Steinhardt, Optimized structures for photonic quasicrystals. *Phys. Rev. Lett.* **101**, 073902 (2008).
27. M. Florescu, S. Torquato, P. J . Steinhardt, Complete band gaps in two-dimensional photonic quasicrystals. *Phys. Rev. B* **80**, 155112 (2009).
28. K. Edagawa, S. Kanoko, M. Notomi, Photonic amorphous diamond structure with a 3d photonic band gap. *Phys. Rev. Lett.*, **100**, 013901 (2008).
29. M. Florescu, S. Torquato, P. J. Steinhardt, Designer disordered materials with large, complete photonic band gaps. *Proc. Natl. Acad. Sci. U.S.A.* **106**, 20658–20663 (2009).
30. S. R. Sellers, W. Man, S. Sahba, M. Florescu, Local self-uniformity in photonic networks. *Nat. Commun.* **8**, 14439 (2017).
31. J. H. Conway, S. Torquato, Packing, tiling, and covering with tetrahedra. *Proc. Natl. Acad. Sci. U.S.A.* **103**, 10612–10617 (2006).
32. J. M. Sullivan, "New tetrahedrally close-packed structures" in *Foams, Emulsions and Their Applications*, P. Zitha, J. Banhart, G. Verbist, Eds. (Delft University of Technology, Delft, 2000).
33. J.-F. Sadoc, R. Mosseri, Quasiperiodic Frank–Kasper phases derived from the square–triangle dodecagonal tiling. *Struct. Chem.* **28**, 63–73 (2017).
34. S. J. Cox, F. Graner, R. Mosseri, J.-F. Sadoc, Quasicrystalline three-dimensional foams. *J. Phys. Condens. Matter* **29**, 114001 (2017).
35. J. M. Sullivan "The geometry of bubbles and foams" in *Foams and Emulsions*, J. F. Sadoc, N. Rivier, Eds. (Springer, Dordrecht, The Netherlands, 1999), pp. 379–402.
36. M. O'Keeffe, "Crystal structures as periodic foams and vice versa" in *Foams and Emulsions*, J. F. Sadoc, N. Rivier, Eds. (Springer, Dordrecht, The Netherlands, 1999), pp. 403–422.

37. J. F. Sadoc, N. Rivier, Eds., *Foams and Emulsions* (Number 354 in NATO Science Series. General Sub-Series E, Applied Sciences, Kluwer Academic Publishers, Dordrecht, 1999).
38. A. Reddy *et al.*, Stable Frank–Kasper phases of self-assembled, soft matter spheres. *Proc. Natl. Acad. Sci. U.S.A.* **115**, 10233–10238 (2018).
39. J. Ricouvier, P. Tabeling, P. Yazhgur, Foam as a self-assembling amorphous photonic band gap material. *Proc. Natl. Acad. Sci. U.S.A.* **116**, 9202–9207 (2019).
40. C. T. Chan, K. M. Ho, C. M. Soukoulis. Photonic band gaps in experimentally realizable periodic dielectric structures. *Europhys. Lett.* **16**, 563–568 (1991).
41. T. Sunada, Crystals that nature might miss creating. *Notices Amer. Math. Soc.* **55**, 205–215 (2008).
42. K. Busch, S. John, Photonic band gap formation in certain self-organizing systems. *Phys. Rev. E* **58**, 3896–3908 (1998).
43. N. Muller, J. Haberko, C. Marichy, F. Scheffold, Silicon hyperuniform disordered photonic materials with a pronounced gap in the shortwave infrared. *Adv. Opt. Mater.* **2**, 115–119 (2014).
44. M. Florescu, K. Busch, J. P. Dowling, Thermal radiation in photonic crystals. *Phys. Rev. B*, **75**, 201101 (2007).
45. H. Miyazaki, M. Hase, H. T. Miyazaki, Y. Kurokawa, N. Shinya, Photonic material for designing arbitrarily shaped waveguides in two dimensions. *Phys. Rev. B* **67**, 235109 (2003).
46. W. Man *et al.*, Isotropic band gaps and freeform waveguides observed in hyperuniform disordered photonic solids. *Proc. Natl. Acad. Sci. U.S.A.* **110**, 15886–15891 (2013).
47. K. A. Brakke, The surface evolver. *Exp. Math.* **1**, 141–165 (1992).
48. S. V. King, Ring configurations in a random network model of vitreous silica. *Nature* **213**, 1112–1113 (1967).
49. M. Maldovan, E. L. Thomas, Diamond-structured photonic crystals. *Nat. Mater.* **3**, 593–600 (2004).
50. S. Johnson, J. Joannopoulos, Block-iterative frequency-domain methods for Maxwell's equations in a planewave basis. *Opt. Express* **8**, 173–190 (2001).
51. W. Setyawan, S. Curtarolo, High-throughput electronic band structure calculations: Challenges and tools. *Comput. Mater. Sci.*, **49**, 299–312 (2010).
52. S. Tsitrin *et al.*, Unfolding the band structure of non-crystalline photonic band gap materials. *Sci. Rep.* **5**, 13301 (2015).
53. M. A. Klatt, P. J. Steinhardt, S. Torquato, Supplementary dataset: Phoamtonic designs yield sizeable 3D photonic band gaps. Zenodo. https://doi.org/10.5281/zenodo.3401635. Deposited 25 October 2019.
54. B. D. Wilts *et al.*, Butterfly gyroid nanostructures as a time-frozen glimpse of intracellular membrane development. *Sci. Adv.* **3**, e1603119 (2017).
55. B. D. Wilts, P. L. Clode, N. H. Patel, G. E. Schröder-Turk, Nature's functional nanomaterials: Growth or self-assembly? *MRS Bull.* **44**, 106–112 (2019).
56. S. Vignolini *et al.*, A 3d optical metamaterial made by self-assembly. *Adv. Mater.* **24**, OP23–OP27 (2012).
57. M. Stefik, S. Guldin, S. Vignolini, U. Wiesner, U. Steiner, Block copolymer self-assembly for nanophotonics. *Chem. Soc. Rev.* **44**, 5076–5091 (2015).
58. P. Ziherl, R. D. Kamien, Soap froths and crystal structures. *Phys. Rev. Lett.* **85**, 3528–3531 (2000).
59. M. Rahm, J.-S. Li, W. J. Padilla, THz wave modulators: A brief review on different modulation techniques. *J. Infrared Millimeter Terahertz Waves* **34**, 1–27, (2013).
60. P. Born, K. Holldack, Analysis of granular packing structure by scattering of THz radiation. *Rev. Sci. Instrum.* **88**, 051802 (2017).
61. H. Zhang, J. Zhang, H. Zhang, Numerical predictions for radar absorbing silicon carbide foams using a finite integration technique with a perfect boundary approximation. *Smart Mater. Struct.* **15**, 759–766 (2006).
62. R. Lemlich, A theory for the limiting conductivity of polyhedral foam at low density. *J. Colloid Interf. Sci.* **64**, 107–110 (1978).
63. L. J. Gibson, Mechanical behavior of metallic foams. *Annu. Rev. Mater. Sci.* **30**, 191–227 (2000).
64. L.-P. Lefebvre, J. Banhart, D. C. Dunand, Porous metals and metallic foams: Current status and recent developments. *Adv. Eng. Mater.* **10**, 775–787 (2008).
65. F. García-Moreno, Commercial applications of metal foams: Their properties and production. *Materials* **9**, 85 (2016).
66. H. X. Zhu, N. J. Mills, J. F. Knott, Analysis of the high strain compression of open-cell foams. *J. Mech. Phys. Solids* **45**, 1875–1904 (1997).
67. J. Stampfl, H. E. Pettermann, M. H. Luxner, "Three-dimensional open cell structures: Evaluation and fabrication by additive manufacturing" in *Fabrication and Characterization in the Micro-Nano Range*, F. A. Lasagni, A. F. Lasagni, Eds. (Springer, Berlin, 2011), vol. 10, pp. 95–117.
68. A. K. Agnihotri, R. Lemlich, Electrical conductivity and the distribution of liquid in polyhedral foam. *J. Colloid Interf. Sci.* **84**, 42–46 (1981).
69. R. Phelan, D. Weaire, E. A. J. F. Peters, G. Verbist, The conductivity of a foam. *J. Phys. Condens. Matter*, **8**, L475–L482 (1996).
70. H. Heesch, F. Laves, Über dünne Kugelpackungen. *Z. Krist.* **85**, 443–453 (1933).
71. S. T. Hyde, M. O'Keeffe, D. M. Proserpio, A short history of an elusive yet ubiquitous structure in chemistry, materials, and mathematics. *Angew. Chem. Int. Ed.*, **47**, 7996–8000 (2008).

PHYSICS